ISSN 1598-0170 (Print)
ISSN 2287-1136 (Online)
http://www.jksii.or.kr

Establishing Best Power Transmission Path using Receiver Based on the Received Signal Strength☆

Jeongsook Eom[1] Heedong Son[1] Yongwan Park[1*]

ABSTRACT

Wireless power transmission (WPT) for wireless charging is currently attracting much attention as a promising approach to miniaturize batteries and increase the maximum total range of an electric vehicle. The main advantage of the laser power beam (LPB) approach is its high power transmission efficiency (PTE) over long distance. In this paper, we present the design of a laser power beam based WPT system, which has a best WPT channel selection technique at the receiver end when multiple power transmitters and single power receiver are operated simultaneously. The transmitters send their transmission channel information via optically modulated laser pulses. The receiver uses the received signal strength indicator and digitized data to choose an optimum power transmission path. We modeled a vertical multi-junction photovoltaic cell array, and conducted an experiment and simulation to test the feasibility of this system. From the experimental result, the standard deviation between the mathematical model and the measured values of normalized energy distribution is 0.0052. The error between the mathematical model and measured values are acceptable, thus the validity of the model is verified.

☞ keyword : wireless power transfer, laser power beaming, vertical multi-junction photovoltaic, received signal strength

1. Introduction

Wireless power transmission (WPT) refers to the transfer of energy or power from one place to another without being connected by wires [1][2]. A major application of WPT is in electronics goods or energy storages such as laptops, tablets, wearable devices, and smartphones [3-5]. There are three main methods of WPT [6-10]. The first method transfers electrical energy employing the phenomenon of mutual induction between two coils operating at the same resonant frequency, the second method is realized with microwave transmitter and receiver, and the third method represents the transfer of electric power using laser technology. A significant drawback of the inductive coupling-based WPT is its short transmission distance [11-14]. Microwave power transmission can cause interference issues in telecommunication infrastructure. The main advantage of the laser power beam (LPB) approach is its high power transmission efficiency (PTE) over long distance [15-16].

We propose a method to select the optimal LPB transmitter (LPBTX) from a group of LPBTXs best-suited to enable a given LPB receiver (LPBRX) to receive the necessary power using an LPB-based WPT system consisting of a single LPBRX and multiple LPBTXs [17][18]. In Section 2, we show the structure and operation of a multichannel WPT system comprising one LPBRX and three LPBTXs. In Section 3, we discuss the modeling and validation of the LPBTX-to-LPBRX charging operation using a vertical multi-junction photovoltaic (VMJ PV) cell array. Simulation result of the operation of the

1 Department of Information and Communication Engineering, Yeungnam University, Gyeongsan, 38541, Korea
* Corresponding author (ywpark@yu.ac.kr)
[Received 29 August 2017, Reviewed 6 September 2017(R2 17 October 2017), Accepted 19 October 2017]
☆ This work was partially supported by the Technology Innovation Program (10054575, The Development of the 8-channel 15f/s grade scanning LiDAR Sensor for autonomous car) funded By the Ministry of Trade, industry & Energy(MI, Korea). This research was also partially supported by the MSIT(Ministry of Science and ICT), Korea, under the ITRC(Information Technology Research Center) support program(IITP-2017-2016-0-00313) supervised by the IITP(Institute for Information & communications Technology Promotion). This work was partially supported by the Technology Innovation Program (No. 10063444, Development of Vehicle-Mounted HUD(Head Up Display) System with Laser Projection) funded By the Ministry of Trade, industry & Energy(MI, Korea).
☆ A preliminary version of this paper was presented at ICONI 2016 and was selected as an outstanding paper.

http://dx.doi.org/10.7472/jksii.2017.18.6.15

proposed system are presented in Section 4.

2. Operation of the Multichannel LPB-based WPT System

The proposed LPB-based WPT system is composed of three LPBTXs and one LPBRX. An LPBTX is equipped with LPB-based WPT to the LPBRX and Wi-Fi communication. An LPBRX performs Wi-Fi communication with all LPBTXs, and converts the LPB received from an LPBTX via an embedded 5×5 VMJ PV cell array into electrical signals or power [19]. Every LPBTX performs Wi-Fi communication with the LPBRX. Upon receiving a request from the LPBRX, each LPBTX emits its own power information in the form of encoded laser pulses using all available LPB channels. The LPBTX, which is selected by the LPBRX as a good match on the basis of its power information, emits an LPB using the designated LPB channel. An LPB channel is an LPB propagation path from an LPBTX to an LPBRX, and its location is expressed by the spherical coordinates of the laser emission angle.

The operation of an LPBTX is divided into standby, detection, and charging phases. In the standby phase, an LPBTX waits for an information request message via Wi-Fi from an LPBRX. On receiving an information request message, it proceeds to the detection phase and sends its unique LPB information encoded with direct sequence optical code division multiple access (DS-OCDMA) [20-23] in a laser beam of Class 1 maximum permissible exposure (MPE), which constitutes a safe level of exposure. The 28-bits LPB information specific to each LPBTX consists of one bit allocated to the initial signal, two bits to the LPBTX ID, seven bits each to the IDs of the two parts (polar angle and azimuthal angle) of the LPB channel available for transmission, eight bits to the maximum output power as one watt, and three bits for a checksum or cyclic redundancy check (CRC). The LPB channel IDs indicate the emission direction of the laser beam on the spherical coordinate system. The CRC, which is used for detecting power transmission errors, can be generated from the device ID, LPB channel ID, and maximum output power ID. The DS-OCDMA system used in this study performs spread spectrum communication based on the 1D unipolar synchronous prime sequence code and digital modulation using the non-return-to-zero on-off keying (NRZ-OOK) technique. Assigning a unique code to each of the three LPBTXs with different two-bit device ID numbers is ensured by using synchronous prime sequence codes with a weight of 5 and code length of 25. An LPBTX sends out sequentially encoded information one after another using one channel each from among the LPB channels available for transmission. Upon completion of LPB information transmission via all available LPB channels, LPBTXs return to the standby phase, and only the one that receives the charging start message from an LPBRX proceeds to the charging phase. An LPBRX analyzes the information sent out by the LPBTXs in the detection phase, selects the optimal LPBTX, and sends a charging start message to the selected LPBTX, thereby designating the LPB channel for the given transmission. The selected LPBTX transmits the maximum power in an LPB using the designated LPB channel. Upon receiving the charging stop message from the LPBRX, the LPBTX stops transmission and returns to the standby phase.

The operation of an LPBRX is divided into standby, detection, and charging phases. In the standby phase, an LPBRX does not receive any LPB. It proceeds to the detection phase and broadcasts an information request message via Wi-Fi whenever a power supply need is sensed. In the detection phase, the LPBRX receives The LPB information from each of the LPBTXs responding to its information request messageis received by a 5×5 VMJ PV cell array, thereby recording the signal strengths. The data thus received are decoded with DS-OCDMA, followed by CRC checksum comparison; the error-free LPB information is saved along with signal strength. Signal strength varies from one incoming LPB to another depending on the distance between LPBTX and LPBRX, the incident angle of the LPB, and the energy distribution in the VMJ PV cell array, because each LPBTX emits its own unique LPB information within the range of Class 1 MPE per pulse. The maximum power receivable from an LPBTX through a particular LPB channel can be calculated using the received channel power indicator (RCPI) signal strength. The LPBRX establishes the optimal power transmission path by selecting the optimal LPBRX and LPB channel on the basis of the size of the maximum power receivable by each LPBRX through each designated LPB channel calculated by substituting the unique LPB information and RCPI of each LPBTX. The LPBRX proceeds then to the charging phase by broadcasting the charging start message to the selected LPBTX along with the information on the designated LPB channel. If the maximum output power of one LPBTX does not meet its power supply need, the LPBRX emits the charging start message to two or more LPBTXs, distributing the total amount of required energy supply among them. When the power supply is drained, an LPBRX receives and analyzes the LPB information sent out by the LPBTXs and selects the optimal LPBTX and LPB channel for power transmission. Each of the three LPBTXs at each crossroad has its own maximum transmission power and LPB channels, and the charging distance and incident angle vary according to the geometric relationship between LPBTX and LPBRX, resulting in different amounts of energy delivered to the LPBRX at each charging event. The LPBRX converts the LPB received through the VMJ PV cell array into electricity for the power supply. If its power supply need is met, the LPBRX broadcasts a charging stop message to the LPBTX. When all LPBTXs stop power delivery, the LPBRX returns to the standby phase and stays in the standby mode until a power supply need is sensed.

3. Mathematical model of a VMJ PV cell array

The type of LPBRX used in this study was equipped with a 5×5 VMJ PV cell array as shown in Figure 1. Daible [24] and zhou [25] proposed a PV cell array model under the Gaussian laser beam condition [26]. In their model, the PV array was a network with dimensions m×n, where m and n represented the number of PV cells in the column and row, respectively. The position of each VMJ PV cell is expressed in the format of PV (i, j), where i and j denote the row and column, respectively, of the VMJ PV cell array. The center of the array is expressed as PV (0, 0) and unique row and column coordinates are assigned to each cell according to the distance from the center cell. The distance between each cell PV (i, j) and the center cell PV (0, 0) is expressed by Di,j and defined by Equation 1.

$$D_{i,j} = \sqrt{(i^2 + j^2)} \qquad \text{Eq. (1)}$$

10mm

PV(-2, 2)	PV(-1, 2)	PV(0, 2)	PV(1, 2)	PV(2, 2)
PV(-2, 1)	PV(-1, 1)	PV(0, 1)	PV(1, 1)	PV(2, 1)
PV(-2, 0)	PV(-1, 0)	PV(0, 0)	PV(1, 0)	PV(2, 0)
PV(-2, -1)	PV(-1, 1)	PV(0, -1)	PV(1, -1)	PV(2, -1)
PV(-2, -2)	PV(-1, -2)	PV(0, -2)	PV(1, -2)	PV(2, -2)

(Figure 1) Coordinates of each PV cell of the 5×5 VMJ PV cell array

1# 0.135	6# 0.287	11# 0.368	16# 0.287	21# 0.135
2# 0.287	7# 0.607	12# 0.779	17# 0.607	22# 0.287
3# 0.368	8# 0.779	13# 1	18# 0.779	23# 0.368
4# 0.287	9# 0.607	14# 0.779	19# 0.607	24# 0.287
5# 0.135	10# 0.287	15# 0.368	20# 0.287	25# 0.135

(Figure 2) Gaussian distribution of $E_{\max}/e^2$ energy relative to the PV (0,0) cell in the 5×5 VMJ PV cell array

In a Gaussian LPB, if the energy value $G_{0,0}$ at PV (0, 0) is taken as the reference, the relative energy value of PV (i, j) at the distance of $D_{i,j}$ is expressed by $G_{i,j} / G_{0,0}$ and defined by Equation 2. Figure 2 shows the energy distribution of $E_{\max} / e^2$ in a 5×5 VMJ PV cell array with an LPB irradiation area of dimensions 56.56 mm × 56.56 mm.

$$\frac{G_{i,j}}{G_{0,0}} = e^{\frac{2D_{i,j}^2}{D_T^2}} \quad \text{Eq. (2)}$$

D_T denotes the diameter of the LPB emitted from the LPBTX at the time of reaching the LPBRX, as defined by Equation 3 [27].

$$D_T = \frac{D_L + \alpha_T R_T}{\cos\theta_T} \quad \text{Eq. (3)}$$

for the following:

- D_L: diameter of the LPB (m)
- α_T: divergence angle of the LPB (rad)
- R_T: distance between LPBTX and LPBRX (m)
- θ_T: angle of the LPB incident to the array (°)

P_R is the sum of the relative energy value ($G_{i,j} / G_{0,0}$) of each cell of the array whose $D_{i,j}$ value is smaller than the LPB diameter. It approximates the constant times (C) of the LPB energy emitted from the LPBTX, and becomes $G_{0,0}$, the energy value of PV (0, 0), which serves as the reference value for each cell's relative energy value.

$$P_R = C \sum_{i=-n}^{i=n} \sum_{j=-n}^{j=n} \frac{G_{i,j}}{G_{0,0}} \left[D_{i,j} \le D_T \right] \quad \text{Eq. (4)}$$

Using the constant c obtained with Equation 4, the energy values of all cells are calculated with $CG_{i,j}$.

Because the VMJ PV cell array's area (A) is a characteristic of an LPBRX, all LPBTXs have the same values for the LPBRX. Therefore, the calculation of energy transfer rate (τ_{sys}) based on the RCPI, which varies from one LPBTX to another in the detection phase, can be simplified to Equation 5.

$$\tau_{sys} = \frac{P_R}{P_{Tclass}} \quad \text{Eq. (5)}$$

With the energy transfer rate calculated on the basis of the RCPI during the detection period, the size (U) of the power receivable by the LPBRX at the maximum output power (P_{Tmax}) can be defined by Equation 6.

$$U = P_{Tmax} \times \tau_{sys} \quad \text{Eq. (6)}$$

To validate a mathematical model of the received energy on an LPBRX with a 5×5 VMJ PV cell array, we conducted an experiment with a 5S1010.4-A555555 from MHGP's standard VMJ PV array product and an MDL-H-808 from Opto Engine LLC. The 5S1010.4-A555555 is suitable for LPB applications requiring power up to 160 W at 975 nm with up to 36% power conversion efficiency. It consists of a 5×5 array of VMJ PV cells with an active cell area of dimensions 52 mm × 50 mm. The MDL-H-808 is an infrared laser module at 808 nm with 6 W output power. Table 1 shows the detailed technical specifications of the MDL-H-808.

〈Table 1〉 Technical specification of the MDL-H-808 laser module

Parameter	Value
Part number	MDL-H-808
Technology	DPSS Laser
Operation mode	Continous wave
Wavelength	808nm
Output power (P_{Tmax})	3 ~ 6W
Beam diameter (D_L)	8mm
Beam divergence (α_T)	3mrad

Table 2 describes the four experimental setups when the laser module MDL-H-808 has located away from the 5S1010.4-A555555 VMJ PV cell array. Figure 3 illustrates the experimental results of the energy distribution when the laser module with 6W average beam power was located at a distance of 16 m from the VMJ PV cell array. The sum of received energy was 1.8145 W. Figure 4 shows the normalized energy distribution relative to the PV (0, 0).

(Table 2) Four experimental setups to validate the mathematical model

Parameter	Setup #1	Setup #2	Setup #3	Setup #4
Average output power (W)	3	4	5	6
Distance between laser and PV array (m)	16	16	16	16
Location of highest irradiance cell	PV (0,0)	PV (0,0)	PV (0,0)	PV (0,0)

1# 0.022	6# 0.050	11# 0.061	16# 0.048	21# 0.022
2# 0.048	7# 0.100	12# 0.130	17# 0.101	22# 0.048
3# 0.061	8# 0.129	13# 0.166	18# 0.130	23# 0.061
4# 0.049	9# 0.105	14# 0.130	19# 0.100	24# 0.048
5# 0.022	10# 0.047	15# 0.062	20# 0.048	25# 0.026

(Figure 3) Received energy when the laser module MDL-H-808 with 6 W average output power was located at a distance of 16 m from the 5S1010.4-A555555 VMJ PV cell array

1# 0.133	6# 0.305	11# 0.369	16# 0.286	21# 0.135
2# 0.288	7# 0.603	12# 0.784	17# 0.610	22# 0.286
3# 0.370	8# 0.779	13# 1	18# 0.780	23# 0.368
4# 0.292	9# 0.633	14# 0.783	19# 0.605	24# 0.288
5# 0.135	10# 0.284	15# 0.371	20# 0.289	25# 0.155

(Figure 4) Energy distribution relative to the PV (0, 0) when the laser module MDL-H-808 with 6 W average output power was located at a distance of 16 m from the 5S1010.4-A555555 VMJ PV cell array

In addition to performance characterization at different intensities, the cell's performance was found to vary about 2.5% for every 10°C change in temperature, as illustrated in Figure 5. It is mounted to 500 ㎛ thick aluminum nitride (AlN) substrates that have a PPC functionality and converts laser beams to electric powers without further additions. We mounted the VMJ PV array onto a commercial off the shelf (COTS) thermoelectric cooler (TEC) with the liquid cooled cold plate to keep the array around 25 °C as possible.

The standard deviation between the mathematical model (Figure 1) and the measured values (Figure 4) are shown in Table 3. As illustrated in Figure 6, the standard deviation of normalized energy distribution relative to the PV(0,0) is 0.0052. It can be seen that the error between the mathematical and measured values is acceptable when considering the factors of the performance difference between the VMJ PV cells and the actual Gaussian LPB; thus, the validity of the irradiance profile model is verified.

(Table 3) Standard deviation of four experimental setups

Parameter	Setup #1	Setup #2	Setup #3	Setup #4
Standard deviation of energy distribution	0.0051	0.0052	0.0054	0.0052
Standard deviation of received power	0.0009	03.0013	0.0017	0.0019

4. Simulation of the WPT system

For simulation, we arranged one LPBRX (R1) and three LPBTXs (T1-T3) with different maximum power levels. Their locations were expressed in terms of x, y, and z axes in a 3D Cartesian coordinate system with the origin at the bottom left corner. An LPBTX is a device that conducts Wi-Fi communication with an LPBRX and transmits signals and energy through an LPB channel using an LPB enabled power output control as requested by the LPBRX. An LPBTX emits DS-OCDMA encoded data in an LPB at the

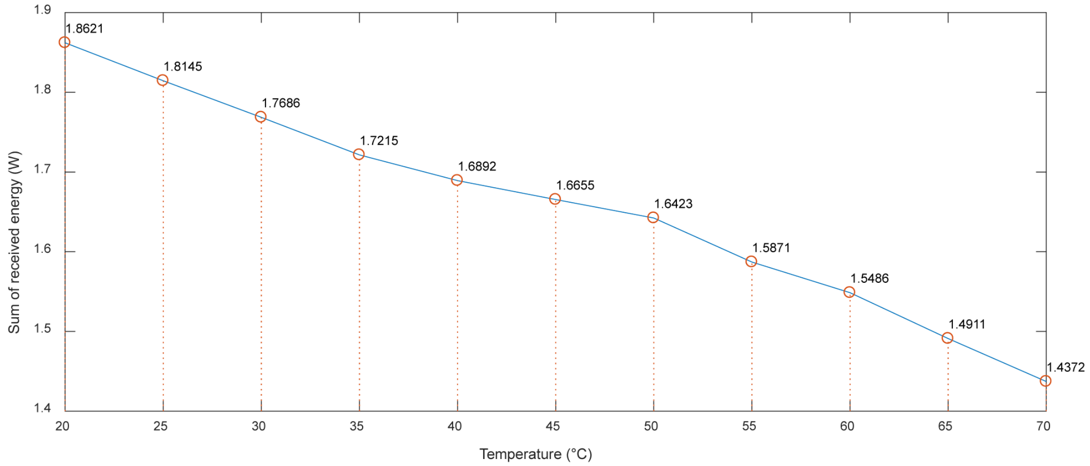

(Figure 5) Relationship between sum of received energy (W) and cell temperature

1# 0.002	6# -0.018	11# -0.001	16# 0.001	21# 0.000
2# -0.001	7# 0.004	12# -0.005	17# -0.003	22# 0.001
3# -0.002	8# 0.000	13# 0.000	18# -0.001	23# 0.000
4# -0.005	9# -0.026	14# -0.004	19# 0.002	24# -0.001
5# 0.000	10# 0.003	15# -0.003	20# -0.002	25# -0.020

(Figure 6) Compared energy distribution between the mathematical model and measured values

constant pulse energy of 6μJ in the detection phase, and an LPB at the maximum output power in the charging phase through the selected LPB channel. It receives power transmission messages via Wi-Fi and carries out operations according to the messages received. The three LPBTXs used in the simulation have different values of maximum transferable power. Table 4 outlines the characteristics of the LPBTXs. The three LPBTXs used in the simulation have different maximum output power and LPB channel characteristics.

(Table 4) Standard deviation of four experimental setups

LPBTX	T1	T2	T3
Maximum output power (W)	60	50	70
Location (x,y,z) (m)	(8,8,10)	(17,8,10)	(8,17,10)
LPB channel range (θ,ϕ)	90°~180°, 0°~360°	90°~180°, 0°~360°	90°~180°, 0°~360°
LPB channel spacing (θ,ϕ)	0.01°, 0.01°	0.01°, 0.01°	0.01°, 0.01°
LPB size (m)	0.001	0.001	0.001
LPB divergence (mrad)	1	1	1

For the simulation, a Wi-Fi-enabled LPBRX is halted at an intersection, waiting for the light to tern green. It is capable of constantly measuring the RCPI and converting the LPB received via the 5×5 VMJ PV cell array into electricity is used as the LPBRX. The LPBRX can broadcast power transmission-related messages to LPBTXs via Wi-Fi and decode and process the DS-OCDMA encoded signals from the LPBTXs received through the 5×5 VMJ PV cell array. Table 5 outlines its characteristics.

(Table 5) Characteristics of LPBRX

LPBRX	R1
Power demand (W)	20
Location (x,y,z) (m)	(6,10,2)
Surface area (m^2)	0.0025
Power conversion efficiency (%)	30

Table 6 presents the results of the simulation as per the algorithm for sequentially selecting the LPBTX in decreasing order of maximum transferable power level by Equation 6. The PTE of each LPBRX is different because the LPB power distribution pattern of the VMJ PV array cell mounted on the LPBRX varies depending on geometric parameters such as the distance between the LPBTX and LPBRX and the incident angle of the LPB. Even when the same amount of power is transmitted by the same LPBTX, one LPBRX may receive an amount similar to the transmitted amount, where another LPBRX may receive only a small portion of the transmitted amount. We used Equations 1-6 and mathematical model of VMJ PV array cell to calculate the RPCI and the maximum deliverable power of each LPB channel. When LPBTXs receive a power request, they send its unique ID code through all LPB channels available for transmission. Each cell displays the information of the LPB channel of the given LPBTX and the RCPI. As defined by Equation 4, the RCPI varies from one LPB channel of an LPBTX to another depending on the strength of the laser beam incident on the LPBRX. If the LPBTX selected first cannot meet the energy demand, the next-best LPBTX is selected, and this LPBTX selection operation continues until the required amount of power is transmitted. In Table 47, LPBRX R1 selected LPBTX T3, which has the greatest amount of power receivable, and was provided with a 20.5079W power supply exceeding its energy demand of 20 W by receiving the power transmitted by LPBTX T4 through the LPB channel (165.26°, 26.57°). As a result, LPBRX R1 was supplied with 102.5% of its respective power supply need.

(Table 6) Established LPB channel information

Parameter		Value
LPBRX	Name	R1
	Power demand (W)	20
LPBTX	Name	T3
	Power emitted (W)	70
	LPB channel (θ,ϕ)	(165.26°, 26.57°)
	Maximum output power point	PV (0,0)
	Power received (W)	20.5079

5. Conclusion

We propose an LPB-based WPT system and demonstrate that it, has the best WPT channel selection technique at the receiver end. We modeled the mathematical normalized energy distribution relative to the center position of the VMJ PV cell array and validated it with four experiments. The receiver of the WPT system calculates the maximum deliverable power based on the RCPI and received power in the detection phase. Moreover, then it can detect its exact transmitter location on its own with different power demands and characteristics of the transmitters. It was confirmed that the energy is transmitted by the LPB. In this study, we constrained the energy receiving channel as three different transmitters, which was necessary for the study of the system with multiple receivers and transmitters. It can be extended to rearrange the PV cell arrays mounted on the receiver to enhance the maximum deliverable power and power transmission efficiency.

Reference

[1] Z. Bi, T. Kan, C. C. Mi, Y. Zhang, Z. Zhao, and G. A. Keoleian, “A review of wireless power transfer for electric vehicles: Prospects to enhance sustainable mobility,” Applied Energy, Vol 179, pp. 413-425, 2016. https://doi.org/10.1016/j.apenergy.2016.07.003

[2] T. C. Rao, and K. Geetha, “Categories, standards and recent trends in wireless power transfer: A survey,” Indian Journal of Science and Technology, Vol. 9, No. 20, 2016. https://doi.org/10.17485/ijst/2016/v9i20/91041

[3] J. Hong, and N. Kim, “The Analysis of Transmission Power Control Model for Energy Efficiency in Body Sensor Systems,” Journal of internet computing and services, Vol. 15, No. 4, pp. 1-8, 2014. https://doi.org/10.7472/jksii.2014.15.4.01

[4] D. Yu, and N. Kim, “Control Packet Transmission Decision Method for Wearable Sensor Systems,” Journal of internet computing and services, Vol. 16, No. 5, pp. 11-17, 2015. https://doi.org/10.7472/jksii.2015.16.5.11

[5] Y. Woo, J. Park, M. Kang, and K. Kwon, "Analysis and Design of Profiling Adaptor for XML based Energy Storage System," Journal of internet computing and services, Vol. 16, No. 5, pp. 29-38, 2015. https://10.7472/jksii.2015.16.5.29

[6] G. Buja, M. Bertoluzzo, and K. N. Mude, "Design and experimentation of WPT charger for electric city car," IEEE Transactions on Industrial Electronics, Vol. 62, No. 12, pp. 7436–7447, 2015. https://doi.org/10.1109/TIE.2015.2455524

[7] F. Baronti, M.-Y. Chow, C. Ma, H. Rahimi-Eichi, and R. Saletti, "E-transportation: the role of embedded systems in electric energy transfer from grid to vehicle," EURASIP Journal on Embedded Systems, Vol. 2016, No. 1. pp. 11-22, 2016. https://doi.org/10.1186/s13639-016-0032-z

[8] S. Li, and C. C. Mi, "Wireless power transfer for electric vehicle applications," IEEE Journal of Emerging and Selected Topics in Power Electronics, Vol. 3, No. 1, pp. 4–17, 2015. https://doi.org/10.1109/JESTPE.2014.2319453

[9] S. Bolonne, A. Chanaka, G. Jayawardhana, I. Lionel, and D. Chandima, "Wireless power transmission for multiple devices," in Moratuwa Engineering Research Conference (MERCon), pp. 242–247, 2016. https://doi.org/10.1109/MERCon.2016.7480147

[10] S. Y. R. Hui, W. Zhong, and C. K. Lee, "A critical review of recent progress in mid–range wireless power transfer," IEEE Transactions on Power Electronics, Vol. 29, No. 9, pp. 4500–4511, 2014. https://doi.org/10.1109/TPEL.2013.2249670

[11] R. Johari, J. V. Krogmeier, and D. J. Love, "Analysis and practical considerations in implementing multiple transmitters for wireless power transfer via coupled magnetic resonance," IEEE Transactions on Industrial Electronics, Vol. 61, No. 4, pp. 1774–1783, 2014. https://doi.org/10.1109/TIE.2013.2263780

[12] K. Lee, and D.-H. Cho, "Diversity analysis of multiple transmitters in wireless power transfer system," IEEE Transactions on Magnetics, Vol. 49, No. 6, pp. 2946–2952, 2013. https://doi.org/10.1109/TMAG.2012.2234132

[13] D. Ahn, and S. Hong, "Effect of coupling between multiple transmitters or multiple receivers on wireless power transfer," IEEE Transactions on Industrial Electronics, Vol. 60, No. 7, pp. 2602–2613, 2013. https://doi.org/10.1109/TIE.2012.2196902

[14] C. R. Valenta, and G. D. Durgin, "Harvesting wireless power: Survey of energy–harvester conversion efficiency in far–field, wireless power transfer systems," IEEE Microwave Magazine, Vol. 15, No. 4, pp. 108–120, 2014. https://doi.org/10.1109/MMM.2014.2309499

[15] T. J. Nugent Jr, and J. T. Kare, "Laser power beaming for defense and security applications," Proc. SPIE 8045, pp. 804514–804514, 2011. https://doi.org/10.1117/12.886169

[16] P. Sprangle, B. Hafizi, A. Ting, and R. Fischer, "High–power lasers for directed–energy applications," Applied Optics, Vol. 54, No. 31, pp. F201–F209, 2015. https://doi.org/10.1364/AO.54.00F201

[17] H. Son, J. Song, and Y. Park, "Establishing Best Optical Channel for Laser Power Beaming," KSII The 8th International Conference on Internet, pp. 1-4, 2016.

[18] J. Eom, G. Kim, and Y. Park, "Establishing optimal power transmission path by the receiver based on the received signal strength with multiple transmitters and receivers," Proc. SPIE 10084, pp. 10084B-1–804514, 2017. https://doi.org/10.1117/12.2251190

[19] A. Massa, G. Oliveri, F. Viani, and P. Rocca, "Array designs for long–distance wireless power transmission: State–of–the–art and innovative solutions," Proceedings of the IEEE, Vol. 101, No. 6, pp. 1464–1481, 2013. https://doi.org/10.1109/JPROC.2013.2245491

[20] C. Goursaud-Brugeaud, A. Julien-Vergonjanne, and J.-P. Cances, "Prime code efficiency in DS–OCDMA systems using parallel interference cancellation," Journal of Communications, Vol. 2, No. 3, pp. 51–57, 2007. https://doi.org/10.4304/jcm.2.3.51-57

[21] G.-C. Yang, and W. C. Kwong, Prime Codes with Applications to CDMA Optical and Wireless

Networks, Artech House, 2002.
[22] W. C. Kwong, and G.-C. Yang, Optical Coding Theory with Prime, CRC Press, 2013.
[23] H. Ghafouri-Shiraz, and M. M. Karbassian, Optical CDMA Networks: Principles, Analysis and Applications, John Wiley & Sons, 2012.
[24] D. E. Daible, Free Space Optical Communication with High Intensity Laser Power Beaming, PhD thesis, Clevel and State University, 2006.
[25] W. Zhou, and K. Jin, “Optimal photovoltaic array configuration under gaussian laser beam condition for wireless power transmission,” IEEE Transactions on Power Electronics, Vol. 32, No. 5, pp. 3662-3672, 2016. https://doi.org/10.1109/TPEL.2016.2583502
[26] R. G. Driggers, C. Hoffman, and R. Driggers, Encyclopedia of Optical Engineering, CRC Press, 2003.
[27] R. Sabatini, and M. A. Richardson, “Airborne laser systems testing and analysis,” Report, NATO Science and Technology Organization, April 2010.

◐ 저 자 소 개 ◑

엄 정 숙(Jeongsook Eom)
1998년 2월 영남대학교 컴퓨터공학과 (공학사)
2002년 2월 영남대학교 정보처리교육학과 (교육학 석사)
2008년 2월 영남대학교 정보통신공학과 공학 박사 수료
2002년 3월~2013년 10월 하드웨어 엔지니어
2013년 10월~현재 영남대학교 정보통신공학과 박사연구생
관심분야 : 자율주행자동차, 레이저 무선 충전, 라이다, 광통신
E-mail : jseom@ynu.ac.kr

손 희 동(Heedong Son)
2017년 8월 영남대학교 정보통신공학과 (공학사)
2017년 9월~현재 영남대학교 정보통신공학과 석사 과정
관심분야 : 레이저 무선 충전, 실내위치측위
E-mail : shd7216@ynu.ac.kr

박 용 완(Yongwan Park)
1989년 2월 뉴욕 주립 버팔로 대학교 전자공학과 (공학 석사)
1992년 6월 뉴욕 주립 버팔로 대학교 전자공학과 (공학 박사)
1994년 1월~1996년 8월 SK텔레콤 기술개발부장
1996년 9월~현재 영남대학교 정보통신공학과 교수
관심분야: 이동통신, 자율주행자동차, 레이저 무선 충전, 라이다, 실내위치측위
E-mail : ywpark@yu.ac.kr